Data Repository Item
Part A: Moraine descriptions

This part of the data repository item provides descriptions and photographs of the moraines in the Muztag Ata and Kongur Shan massifs that were examined in this study. The moraines are listed and described by glacial stage (oldest to youngest).

Karasu glacial stage moraines (m_1)

The moraines of the Karasu are highly degraded and denuded, and are present on till benches that contain scattered surface boulders. Till comprises numerous bullet-shaped and edge-rounded boulders with occasional striations. Surface boulders are sparse and some meter-size boulders are weathered flat to the surface of the landform. The locations of each moraine and an explanation of nomenclature for numbering the moraines are described in the paper.

Moraine m_{1E}: View NE at the moraines on the SW flank of the Muztag Ata. The moraine stretches ~ 20 km by ~10 km and is >100 m thick in its exposed marginal section. It is essentially a giant lobe of multiple moraines ridges that rise >200 m above the foreland. There are three valley glaciers in the upvalley of the deposit, which advanced and joined to form a piedmont glacier during to produce this extensive area of moraine ridges. This moraine complex is composed of massive matrix-supported boulder diamict.

Moraine m_{1E}: View looking SW at a typical gneiss boulder on a moraine on the SW flank of Muztag Ata. The boulder is ~1 m high and 1.6 m wide. The surface of the boulder has many weathering pits as deep as ~10 cm and looks dark due to surface weathering. The top left corner of the boulder surface has still polished surface.

Subaxh Glacial Stage Moraines

Subaxh glacial stage moraines are present near the frontal slopes of the massifs and along the slopes of topographic highs. Numerous highly weathered surface boulders are present on their surfaces, reaching ~10 m in diameter. Moraine ridges generally rise 10-15 m above the surrounding surface. In some areas the moraines are preserved against small topographic highs (usually ridges) to form subdued ridges.

Moraine m_{2A}: View looking NE at a moraine below Olimde Glacier with Kongur Shan in the background. The surface comprises undulating hummocks with scattered boulders. Most of boulders have ≤15cm-deep weathering pits. The moraine rises >150 m above moraine of the Olimde glacial stage.

Moraine m_{2B}: View looking E at a piedmont moraine present behind the village of Subaxh, located ~5 km from the Yangbuk Glacier. The moraine ridge rises ~ 6 m higher than the surrounding surface and is sharp-crested, suggesting that this formed during a significant glacial advance. Most of the boulders consist of gneiss, which have 5 cm-deep weathering pits. This piedmont type of moraine rising above gently undulating topography, which is very characteristic of the Subaxh glacial stage moraines.

Moraine m_{2C}: View N at a moraine ridge in the Kartamak Valley. The tent is located in a depression that is ~10 m lower than the moraine ridge (seen in the background). Up valley of the terminal ridge of this moraine, the surface of the deposit is hummocky. The boulders are relatively small (<2 m in height) and they have many weathering pits on their surfaces. Most of the boulders consist of meta-sedimentary rock and gneiss.

Moraine m_{2D}: View looking SE at a till drift surface on the southwestern flank of the Muztag Ata. The car provides scale. The flat boulders in the front of the car show that much of surface of this landform has been eroded. Few boulders stand >1 m higher than the surrounding surface.

Moraine m_{2D}: View of piedmont glacial deposit that was sampled for a TCN surface exposure depth-profile dating. The deposit comprises a massive matrix-supported diamict containing cobbles and boulders. The matrix consists of coarse sand with small pebbles. The deposit is slightly cemented by calcite in places.

Moraine m_{2G}: View S at morainic deposits on the eastern flank of Kongur Shan between the Ting and Kongurjiubie glaciers. The ridge of the deposit is perpendicular to main valley direction, suggesting that the moraine was formed by glacier advance from Kongur Shan. The sediments comprise massive clast-supported, diacmict underlain by stratified fluvial sands. The boulders are extremely weathered and few stand tall.

Moraine m_{2H}: View N at a granite boulder on a moraine of the Ting Glacier. The boulder is ~1.2 m-high and exhibits cavernous weathering. The surface of moraine is very hummocky and it is difficult to track a continuous ridge line, but traces of ridges trend perpendicular to valley, suggesting that this is an latero-frontal moraine.

Olimde Glacial Stage Moraines

Olimde glacial stage moraines comprise multiple sets of well-formed latero-frontal moraines. Each set of moraines generally comprises composite ridges. The moraines have sharp crests and rise several tens of meters above the valley floors, with steep slopes that commonly exceeded 30^{o}. Their surfaces are armored with meter-size angular to subangular boulders that exhibit little/no evidence of weathering. Exposures reveal that the moraines comprise massive matrix-supported diamict. The moraines have abundant meter-size surface boulders, many of which have mm-size weathering pits and are slightly exfoliated. Exposures confirm that the moraines comprise massive matrix-supported diamicts with edge round clasts, some of which have stiations. Some of these youngest moraines have become rock glacierized.

Moraines m_{3A} and m_{4A}: View N at moraine ridges near the confluence of the Olimde and Kengxuwar river valleys. Half-obscured ridge in the far left of the picture is moraine m_{3A} and the little subdued ridge a moraine m_{4A}. Moraine m_{3A} is located ~20 m away from m_{4A} along Olimde Valley. Each of the moraine ridges stretch for ~100 m downvalley. Most of the boulders stand high on the ridges or on the ridge slopes. The boulders consist mainly of meta-sedimentary rock, which was derived from northwestern flank of Muztag Ata massif. The moraines trend parallel to Olimde Valley, indicating that this is a lateral moraine.

Moraine m_{5A}: View E at boulders on a lateral moraine ridge that runs parallel to the length of the Olimde Valley. The Olimde glacier is apparent in the background.

Moraine m_{6A}, m_{7A} and m_{8A}: View E at a flight of moraines in Olimde Valley on the northwestern flank of Muztag Ata. The Olimde Glacier is apparent in the background.

The three ridges are moraines m_{6A}, m_{7A}, and m_{8A} (from lowest to upper). The moraines are all sharp-crested and very distinctive and form enclosed loops.

Moraines m_{3C}, m_{4C}, and m_{5C}: View SW at moraines below the snout of Kartamak Glacier. All of the moraines are sharp-crested and loop around the glacier. The ridge of m_{5C} is shorter than those of m_{3C} and m_{4C}. Moraine m_{3C} is shown in more detail in the next photograph.

Moraine m_{3C}: Close-up of moraine ridge in the Kartamak valley. The ridge rises >20 m above the surrounding lowland. The boulders have small weathering pits on their surfaces and are coated with lichen. Some of the boulders are reddish in color due to surface weathering.

Moraine m_{4C}: View W at moraine ridge ~500 m downvalley from the Kartamak Glacier. The ridge is sharp-crested and rises ~10 m above the surrounding lowland. The ridge loops around the present glacier to form an impressive latero-frontal moraine.

Moraine m_{5C}: View E at a sharp-crested moraine on the western flank of Muztag Ata. The Kartamak Glacier is present in the background. The moraine ridge rises ~20 m above the surrounding lowland and the central portion of the ridge is eroded by a stream.

Moraine $m_{6C'}$: View N at rock-glacierized moraine of the Kartamak Glacier. This moraine rises >30 m above the surrounding surface. The boulders on the moraine are very fresh and exhibit little evidence of weathering, but are covered by lichen. The tents provide a scale.

Moraine m_{3F}: View NE at hummocky moraine to the north of Kara Kol (lake). This extensive moraine field was formed by the advance of the Jangmanjiar Glacier (seen in the background). A horse provides a scale.

Moraine m_{6C}: View S at an impressive latero-frontal moraine that encloses the Kartamak Glacier. The moraine is very steep (>30º) and rises ~100 m above the surrounding topography. The boulders are very fresh and exhibit no evidence of weathering.

Moraine m_{3F}: A close up view of moraine m_{3F}. The hummocky surface suggests that this portion belonged to the inner portion (not the terminal portion) of the moraine. The frontal portion of the moraine is sharp-crested, and arc-shaped in plan, as shown in the following photograph.

Moraine $m_{3F'}$: View S at the moraine ridge of $m_{3F'}$. The ridge rises ~5 m above the surrounding surface. This moraine was formed by the advance of the Kongurjiubie Glacier. The boulders are more than 2 m tall and 1.5 m wide and consist mainly of gneiss and granite.

Moraine m_{3H}: View N at boulders on the moraine ridge formed by the advance of the Ting Glacier. The boulders are dark in color and covered with lichen. Some have weathering pits that reach ~4 cm in depth. The ridge is degraded and has a very gentle surface. However, the ridge rises ~3 m above the surrounding surface and thus it is easy in the very field to trace the ridges. In addition, the ridge runs approximately perpendicular (E-W) to the main valley direction, confirming that this landform is a moraine that formed by the advance of the Ting Glacier.

Moraine m_{4H}: View E at a boulder on moraine ridge in the Ting Valley. The boulder is ~1.1 m tall and 1.6 m wide. This is only slightly weathered and only covered by dark-coating due to surface weathering. Striations are present on its surface. The glacier advanced from the bottom to the top of the photograph.

Moraine m_{5H}: View N at boulders on the moraine ridge formed by advance of Ting Glacier. The moraine ridge is sharp-crested and rises ~10 m above the surrounding surface. The boulders on the moraine are only slightly weathered and some of them are striated.

Moraine m_{6H}: View S at boulders on a moraine ridge ~500 m from the snout of the Ting Glacier. The moraine ridge is sharp-crested and the boulders are only very slightly weathered. The surfaces of the boulders are dark and striated.

Moraine m_{7H}: View of rock-glacierized moraine south of the Ting Glacier. The moraine ridge is very steep (~20º) and high (>> 120 m). A younger moraine is present above this main moraine likely to form during the Little Ice Age.

Moraine m_{3I}: View W at a lateral moraine formed by the debris-covered Karayalak Glacier. The ridge is sharp-crested and rises 15-20 m above the surrounding surface. The boulders are very fresh and have few weathering pits on their surfaces, but are covered with lichen.

Part B: Calculations for terrestrial cosmogenic nuclide surface exposure ages for the Muztag Ata – Kongur Shan region of western Tibet based on different scaling models.

The production of in situ terrestrial cosmogenic nuclides (TCN) is dependent on the flux of cosmic rays that reaches the Earth's surface. The cosmic ray flux has varied spatially (both latitude and altitude) and temporally in association with geomagnetic field intensity and atmospheric pressure throughout the Quaternary (Lal, 1991). Specifically, it is well documented from many independent proxy records that the Earth's geomagnetic field strength fluctuated considerably throughout the Quaternary (Ohno and Hamano, 1992; Guyodo and Valet, 1999; Yang et al., 2000). However, there is currently much debate regarding the appropriate scaling models and geomagnetic corrections for TCN production to calculate TCN ages, especially for low latitude and high altitude regions (e.g. Pigati and Lifton, 2004; and Staiger et al., 2007). To assess the affects of using different scaling models and geomagnetic corrections on a modeled TCN ages, we calculated our TCN ages using five different schemes. For this study, we used several models built on various scaling methods for change in geomagnetic field intensity, focusing on the last 30 ka mostly well documented and relevant to most of the samples we measured. Because the sampled area is relatively small (~100 km^2), all the values are calculated for the middle of the study area (38.343°N, 75.013°E, 4110 m asl) using CRONOUS Earth 2 (http://hess.ess.washington.edu/math/).

Building on various scaling models, we calculated the modeled exposure ages (Table DR 1), age difference between different schemes (Fig. DR 1) and variations in production rate for the study area (Fig. DR 2). Ultimately, we plotted all the apparent glacial events induced from the various models (Fig. DR 3). Our modeling results show limited geomagnetic effects on exposure ages, indicating that maximum age difference for the Holocene samples among the various methods is less than 10 % and the samples for 10-30 ka is less than 15. Furthermore, when probability plots for each set of moraines are plotted, the apparent difference between age models is less obvious and significant. On the basis of these results, we would assume that our modeled surface exposure ages are reliable enough to differentiate each glacial advance for the Late-glacial and the Holocene period. However, synchroniety with other proxy records still needs more independent study owing to uncertainties in terrestrial cosmogenic production rate until now.

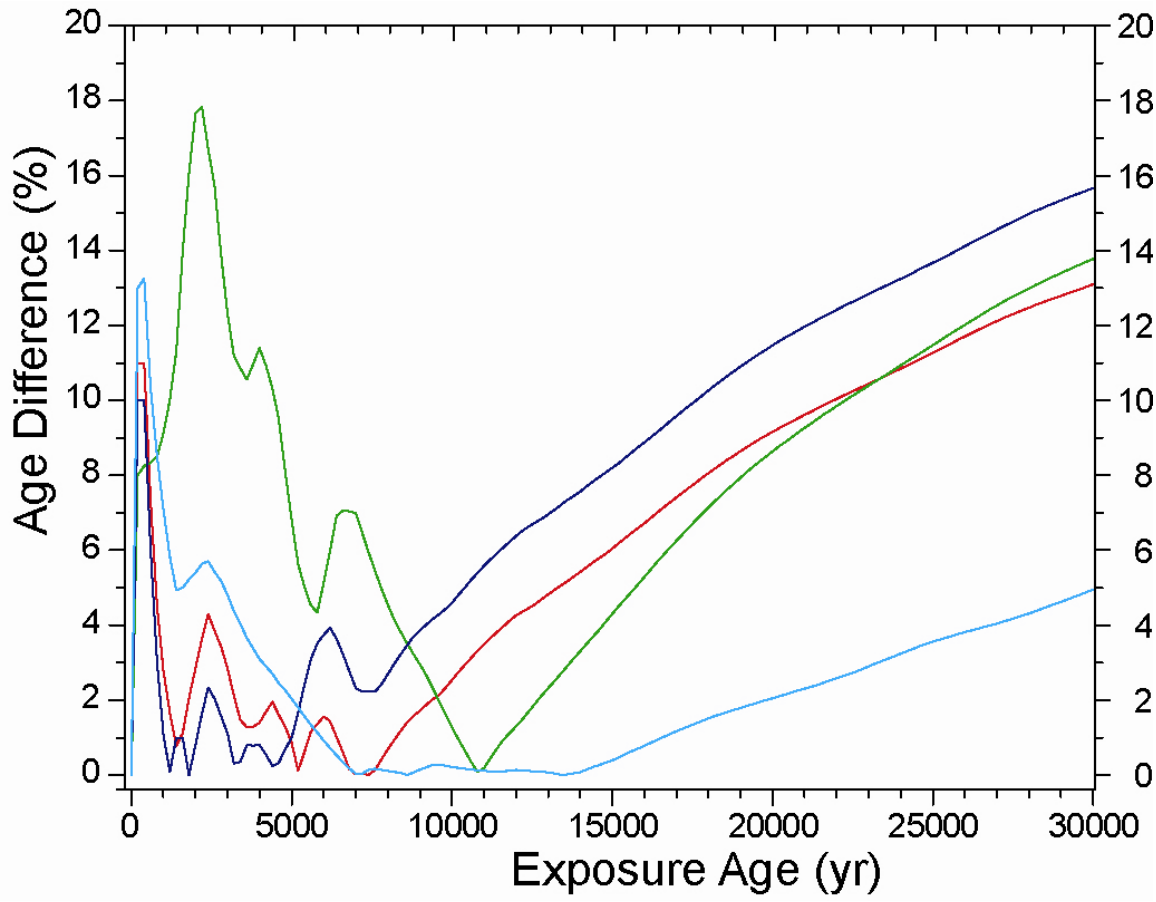

Figure DR1. Percentage exposure age difference over the last 30 ka between time constant scaling method (Lal, 1991; Stone, 2000) and various time-varying scaling schemes at the location (38.343°N, 75.013°E, 4110 m asl) in the middle of the study area. red, Desilets and Zreda (2003,2006); green, Dunai (2001); blue, Lifton et al. (2005); cyan, time-dependent adaptation of Lal(1991)/Stone(2000).

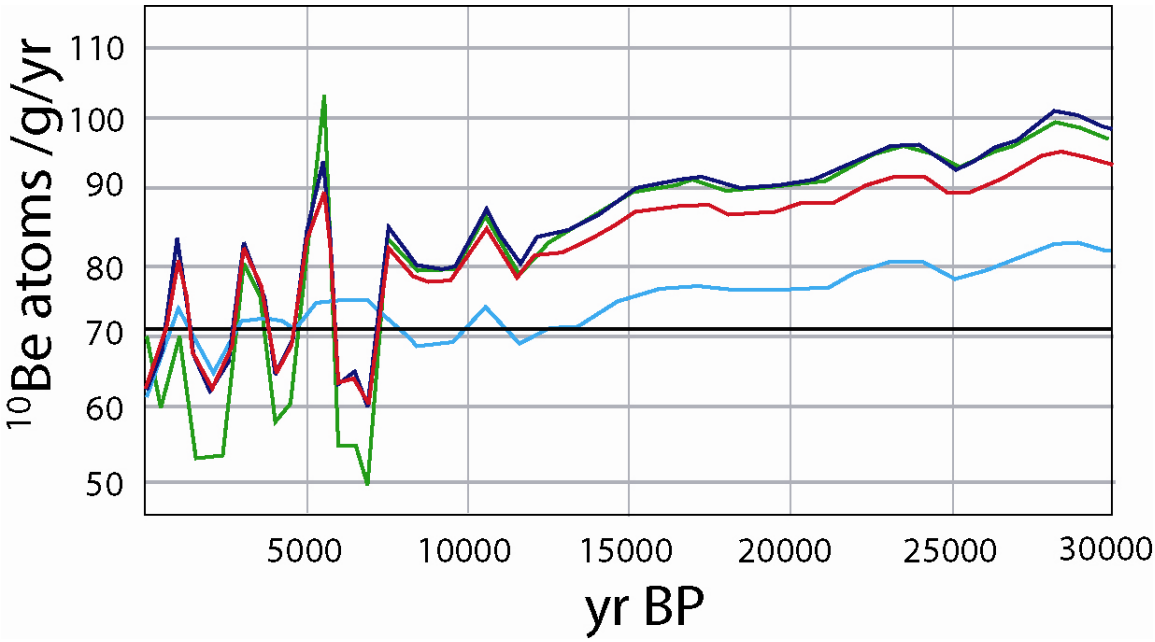

Figure DR2. Consequent changes in Be-10 production rates ages generated from various scaling schemes at the location (38.343°N, 75.013°E, 4110 m asl) in the middle of the study area. The non-time-dependent production rate derived from the Lal(1991)/Stone(2000) scaling scheme is shown by the black line. Time-dependent production: red, Desilets, et al. (2003,2006); green, Dunai (2001); blue, Lifton et al. (2005); cyan, time-dependent adaptation of Lal(1991)/Stone(2000).

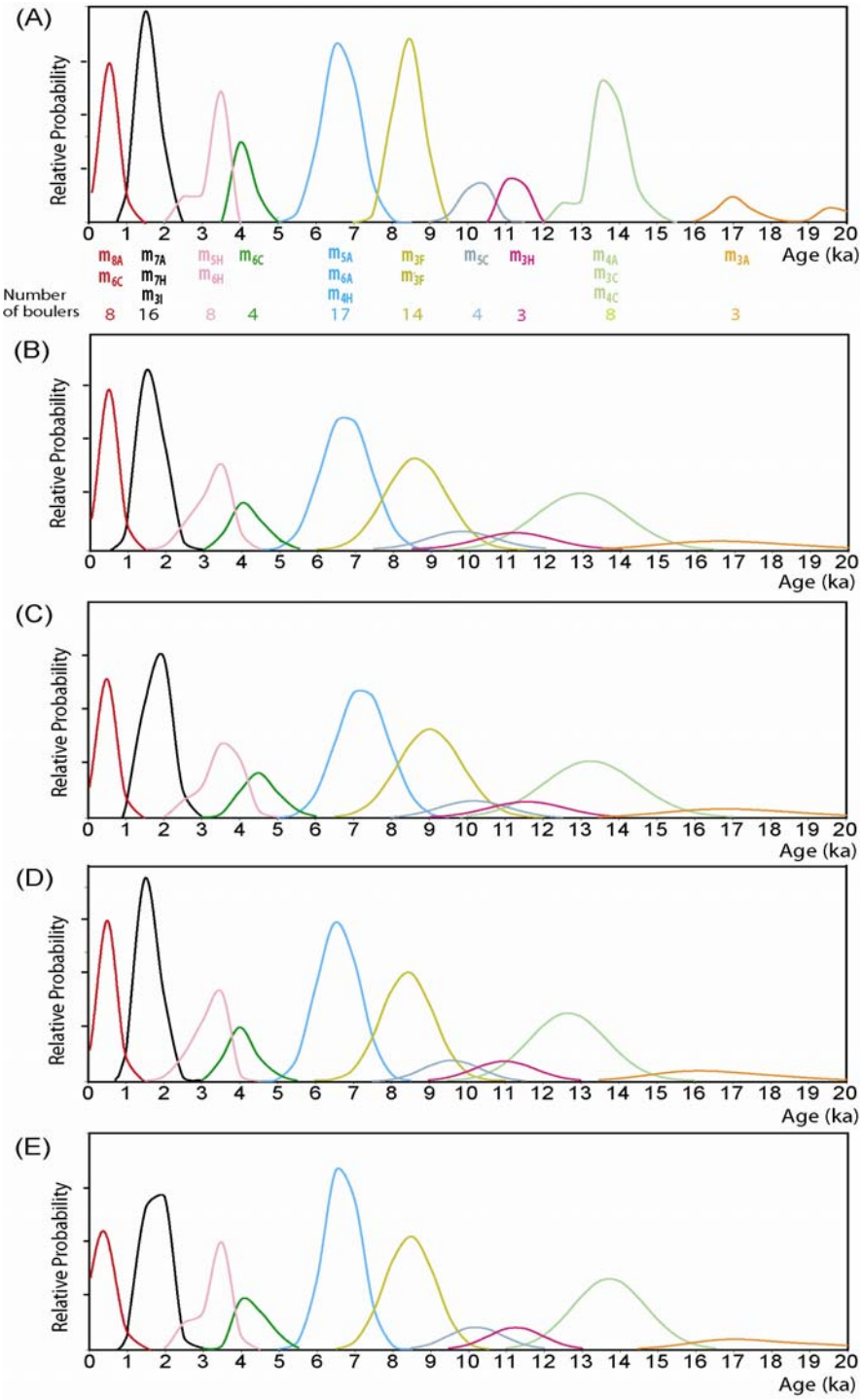

Figure DR3. Probability curves of various scaling schemes for rapid climate changes throughout the Late-glacial and the Holocene. (A) is produced from the non-time-dependent production rate derived from the Lal(1991)/Stone(2000) scaling scheme. (B) is from Desilets, et al. (2003, 2006). (C) is from Dunai (2001). (D) is from Lifton et al. (2005). (E) is from time-dependent adaptation of Lal(1991)/Stone(2000).

TABLE DR1. COSMOGENIC ^{10}BE EXPOSURE AGES FROM VARIOUS SCALING SCHEMES.

Sample name	Constant production model* Lal, 1991 & Stone, 2000 (ka)	Time- varying production model† Desilets and Zreda , 2003; 2006 (ka)	Age difference (%)§	Dunai, 2001 (ka)	Age difference (%)	Lifton et al., 2005 (ka)	Age difference (%)	Lal, 1991 & Stone, 2000 (ka)	Age difference (%)
MUST-1	8.7 ± 0.8	8.8 ± 1.1	1.2	9.3 ± 1.1	5.9	8.7 ± 0.9	0.9	8.8 ± 0.8	0.1
MUST-2	8.7 ± 0.8	8.8 ± 1.1	1.3	9.2 ± 1.1	6.1	8.6 ± 0.9	0.8	8.7 ± 0.8	0.1
MUST-3	8.9 ± 0.8	9.0 ± 1.1	1.0	9.4 ± 1.2	5.6	8.8 ± 0.9	1.1	9.0 ± 0.8	0.2
MUST-4	8.6 ± 0.8	8.7 ± 1.1	1.2	9.1 ± 1.1	6.0	8.5 ± 0.9	0.9	8.6 ± 0.8	0.0
MUST-5	8.6 ± 0.8	8.7 ± 1.1	1.3	9.2 ± 1.1	6.1	8.6 ± 0.9	0.8	8.6 ± 0.8	0.1
MUST-6	8.5 ± 0.8	8.6 ± 1.1	1.4	9.1 ± 1.1	6.3	8.5 ± 0.9	0.7	8.5 ± 0.8	0.0
MUST-7	8.9 ± 0.8	9.1 ± 1.1	2.1	9.5 ± 1.2	6.7	8.9 ± 0.9	0.1	8.9 ± 0.8	0.2
MUST-8	8.7 ± 0.8	8.9 ± 1.1	2.2	9.3 ± 1.1	6.9	8.7 ± 0.9	0.2	8.7 ± 0.8	0.1
MUST-9	8.4 ± 0.8	8.6 ± 1.1	2.5	9.0 ± 1.1	7.4	8.4 ± 0.9	0.5	8.4 ± 0.7	0.0
MUST-10	7.8 ± 0.7	8.1 ± 1.0	3.2	8.5 ± 1.0	8.4	7.9 ± 0.8	1.3	7.8 ± 0.7	0.1
MUST-11	7.9 ± 0.7	8.1 ± 1.0	3.3	8.5 ± 1.0	8.5	8.0 ± 0.8	1.4	7.8 ± 0.7	0.1
MUST-12	8.2 ± 0.8	8.5 ± 1.0	2.8	8.9 ± 1.1	7.8	8.3 ± 0.9	0.9	8.2 ± 0.7	0.0
MUST-13	8.1 ± 0.8	8.3 ± 1.0	2.9	8.7 ± 1.1	8.0	8.2 ± 0.9	1.0	8.1 ± 0.7	0.0
MUST-14	8.2 ± 0.7	8.4 ± 1.0	2.7	8.8 ± 1.1	7.8	8.2 ± 0.8	0.8	8.2 ± 0.7	0.0
MUST-15	125.0 ± 11.7	100.2 ± 12.5	19.8	97.9 ± 12.2	21.7	96.3 ± 10.1	22.9	111.7 ± 10.2	10.6
MUST-16	106.9 ± 9.9	86.7 ± 10.8	18.9	84.6 ± 10.4	20.9	83.0 ± 8.6	22.3	97.0 ± 8.7	9.3
MUST-17	69.1 ± 6.3	56.5 ± 7.0	18.1	55.4 ± 6.8	19.8	53.8 ± 5.5	22.1	63.3 ± 5.7	8.4
MUST-18	44.1 ± 4.0	36.9 ± 4.5	16.3	36.4 ± 4.5	17.4	35.7 ± 3.7	19.0	40.3 ± 3.6	8.6
MUST-19	135.0 ± 12.6	107.3 ± 13.4	20.5	104.8 ± 13.0	22.4	102.9 ± 10.7	23.8	119.9 ± 10.9	11.2
MUST-20	89.0 ± 8.4	72.2 ± 9.1	18.9	70.6 ± 8.8	20.6	69.1 ± 7.3	22.3	81.2 ± 7.5	8.8
MUST-21	6.9 ± 0.6	7.0 ± 0.9	1.7	7.5 ± 0.9	8.8	6.8 ± 0.7	0.6	6.9 ± 0.6	0.1
MUST-22	6.4 ± 0.6	6.5 ± 0.8	1.0	7.0 ± 0.9	8.8	6.3 ± 0.7	1.6	6.5 ± 0.6	0.5
MUST-23	6.3 ± 0.6	6.3 ± 0.8	0.6	6.8 ± 0.8	8.5	6.1 ± 0.6	1.9	6.3 ± 0.6	0.7
MUST-24	6.4 ± 0.6	6.5 ± 0.8	0.9	7.0 ± 0.9	8.8	6.3 ± 0.7	1.6	6.4 ± 0.6	0.5
MUST-25	6.7 ± 0.6	6.8 ± 0.8	1.5	7.3 ± 0.9	8.8	6.6 ± 0.7	1.1	6.7 ± 0.6	0.3
MUST-26	6.7 ± 0.6	6.8 ± 0.8	1.6	7.3 ± 0.9	8.8	6.6 ± 0.7	0.9	6.7 ± 0.6	0.3

MUST-27	6.4 ± 0.6	6.3 ± 0.8	0.4	6.8 ± 0.8	7.6	6.2 ± 0.6	3.0	6.4 ± 0.6	0.6
MUST-28	6.8 ± 0.6	6.8 ± 0.8	0.4	7.3 ± 0.9	7.7	6.6 ± 0.7	2.1	6.8 ± 0.6	0.2
MUST-29	6.5 ± 0.6	6.5 ± 0.8	0.1	7.0 ± 0.9	7.7	6.4 ± 0.7	2.6	6.6 ± 0.6	0.4
MUST-30	7.0 ± 0.6	7.0 ± 0.9	0.6	7.5 ± 0.9	7.7	6.8 ± 0.7	1.7	7.0 ± 0.6	0.1
MUST-31	6.4 ± 0.6	6.4 ± 0.8	0.3	6.9 ± 0.8	7.7	6.2 ± 0.6	2.9	6.4 ± 0.6	0.5
MUST-32	1.7 ± 0.2	1.7 ± 0.2	1.9	2.0 ± 0.3	15.5	1.7 ± 0.2	0.2	1.8 ± 0.2	5.2
MUST-33	1.8 ± 0.2	1.8 ± 0.2	2.2	2.1 ± 0.3	16.2	1.8 ± 0.2	0.2	1.9 ± 0.2	5.2
MUST-34	1.8 ± 0.2	1.9 ± 0.2	2.3	2.1 ± 0.3	16.5	1.8 ± 0.2	0.3	1.9 ± 0.2	5.2
MUST-35	2.1 ± 0.2	2.2 ± 0.3	3.4	2.5 ± 0.3	18.4	2.1 ± 0.2	1.3	2.2 ± 0.2	5.6
MUST-36	1.7 ± 0.2	1.8 ± 0.2	1.4	2.0 ± 0.3	15.1	1.7 ± 0.2	0.7	1.8 ± 0.2	5.1
MUST-37	1.7 ± 0.2	1.7 ± 0.2	1.2	2.0 ± 0.2	14.7	1.7 ± 0.2	0.9	1.8 ± 0.2	5.1
MUST-38	1.7 ± 0.2	1.7 ± 0.2	1.1	1.9 ± 0.3	14.5	1.7 ± 0.2	1.0	1.8 ± 0.2	5.1
MUST-39	0.4 ± 0.1	0.4 ± 0.1	10.6	0.4 ± 0.1	7.4	0.4 ± 0.1	9.3	0.4 ± 0.1	13.3
MUST-40	0.8 ± 0.1	0.8 ± 0.1	3.7	0.9 ± 0.1	7.7	0.8 ± 0.1	2.2	0.9 ± 0.1	8.3
MUST-41	0.5 ± 0.1	0.6 ± 0.1	8.7	0.5 ± 0.1	7.5	0.5 ± 0.1	7.5	0.6 ± 0.1	11.8
MUST-42	17.4 ± 1.6	16.5 ± 2.1	5.2	16.6 ± 2.1	4.1	16.1 ± 1.7	7.3	17.1 ± 1.6	1.2
MUST-43	16.9 ± 1.5	16.0 ± 2.0	4.8	16.2 ± 2.0	3.6	15.7 ± 1.6	6.9	16.7 ± 1.5	1.0
MUST-44	19.7 ± 1.8	18.4 ± 2.3	6.5	18.5 ± 2.3	5.8	18.0 ± 1.8	8.7	19.3 ± 1.7	1.9
MUST-45	13.7 ± 1.2	13.2 ± 1.6	3.6	13.5 ± 1.6	1.4	12.9 ± 1.3	5.7	13.7 ± 1.2	0.0
MUST-46	13.9 ± 1.3	13.4 ± 1.7	3.7	13.7 ± 1.7	1.6	13.1 ± 1.4	5.8	13.9 ± 1.3	0.0
MUST-47	13.9 ± 1.3	13.4 ± 1.6	3.7	13.7 ± 1.7	1.5	13.1 ± 1.3	5.8	13.9 ± 1.2	0.0
MUST-48	367.1 ± 37.4	294.4 ± 39.1	19.8	286.4 ± 37.8	22.0	280.9 ± 31.3	23.5	324.6 ± 32.0	11.6
MUST-49	208.5 ± 19.2	169.5 ± 21.1	18.7	164.9 ± 20.5	20.9	161.4 ± 16.7	22.6	185.7 ± 16.6	10.9
MUST-50	261.0 ± 24.5	209.6 ± 26.4	19.7	204.0 ± 25.6	21.9	199.4 ± 20.9	23.6	231.3 ± 21.1	11.4
MUST-88	151.5 ± 13.9	123.4 ± 15.3	18.6	120.8 ± 14.9	20.3	118.1 ± 12.1	22.0	134.1 ± 11.9	11.5
MUST-89	156.4 ± 15.4	127.4 ± 16.4	18.5	124.6 ± 16.0	20.3	121.8 ± 13.2	22.1	138.5 ± 13.3	11.4
MUST-52	0.1 ± 0.0	0.2 ± 0.2	8.4	0.2 ± 0.1	4.9	0.2 ± 0.1	7.0	0.2 ± 0.1	13.3
MUST-53	0.4 ± 0.1	0.4 ± 0.1	8.6	0.4 ± 0.1	5.6	0.4 ± 0.1	7.2	0.4 ± 0.1	13.3
MUST-54	0.3 ± 0.1	0.3 ± 0.1	8.7	0.3 ± 0.1	5.9	0.3 ± 0.1	7.3	0.3 ± 0.1	13.5
MUST-55	0.6 ± 0.1	0.6 ± 0.1	6.1	0.6 ± 0.1	5.8	0.6 ± 0.1	4.7	0.6 ± 0.1	11.0
MUST-56	0.5 ± 0.1	0.5 ± 0.1	8.4	0.5 ± 0.1	5.7	0.5 ± 0.1	7.2	0.5 ± 0.1	12.7
MUST-57	14.1 ± 1.3	13.1 ± 1.6	6.9	13.4 ± 1.6	4.8	12.8 ± 1.3	9.1	14.1 ± 1.2	0.1
MUST-58	13.7 ± 1.2	12.8 ± 1.6	6.4	13.1 ± 1.6	4.2	12.5 ± 1.3	8.6	13.7 ± 1.2	0.1

MUST-59	13.6 ± 1.3	12.8 ± 1.6	6.3	13.1 ± 1.6	4.0	12.5 ± 1.3	8.5	13.6 ± 1.2	0.0
MUST-60	12.7 ± 1.1	11.9 ± 1.5	5.7	12.3 ± 1.5	3.0	11.7 ± 1.2	7.9	12.7 ± 1.1	0.1
MUST-61	14.7 ± 1.3	13.7 ± 1.7	6.8	14.0 ± 1.7	4.9	13.4 ± 1.4	9.0	14.6 ± 1.3	0.3
MUST-62	17.4 ± 1.7	16.2 ± 2.0	6.9	16.4 ± 2.1	5.8	15.8 ± 1.7	9.1	17.2 ± 1.6	1.3
MUST-63	24.9 ± 2.3	22.3 ± 2.7	10.4	22.3 ± 2.7	10.6	21.7 ± 2.2	12.8	24.1 ± 2.2	3.5
MUST-64	23.2 ± 2.1	21.0 ± 2.6	9.6	21.0 ± 2.6	9.5	20.4 ± 2.1	12.0	22.5 ± 2.0	2.9
MUST-65	75.4 ± 6.9	61.9 ± 7.6	18.0	60.8 ± 7.4	19.5	59.3 ± 6.1	21.4	68.8 ± 6.1	8.8
MUST-66	49.0 ± 4.4	40.3 ± 4.9	17.8	39.8 ± 4.8	18.9	38.9 ± 3.9	20.7	44.3 ± 3.9	9.7
MUST-86	23.8 ± 2.2	21.4 ± 2.6	9.8	21.4 ± 2.6	9.8	20.9 ± 2.1	12.2	23.0 ± 2.0	3.1
MUST-67	13.7 ± 1.3	12.9 ± 1.6	6.0	13.2 ± 1.6	3.8	12.6 ± 1.3	8.2	13.7 ± 1.3	0.1
MUST-68	13.5 ± 1.2	12.7 ± 1.5	5.8	13.0 ± 1.6	3.5	12.4 ± 1.3	8.0	13.5 ± 1.2	0.0
MUST-69	14.2 ± 1.3	13.3 ± 1.6	6.2	13.6 ± 1.7	4.1	13.0 ± 1.3	8.4	14.2 ± 1.3	0.2
MUST-70	13.4 ± 1.2	12.6 ± 1.5	5.8	12.9 ± 1.6	3.4	12.3 ± 1.3	7.9	13.4 ± 1.2	0.0
MUST-71	13.6 ± 1.2	12.8 ± 1.6	5.9	13.1 ± 1.6	3.6	12.5 ± 1.3	8.1	13.6 ± 1.2	0.0
MUST-72	11.4 ± 1.0	10.8 ± 1.3	4.8	11.2 ± 1.4	1.7	10.6 ± 1.1	6.9	11.4 ± 1.0	0.1
MUST-73	9.8 ± 0.9	9.5 ± 1.2	3.4	9.9 ± 1.2	0.6	9.3 ± 0.9	5.5	9.8 ± 0.9	0.2
MUST-74	10.3 ± 0.9	9.9 ± 1.2	3.8	10.3 ± 1.3	0.2	9.7 ± 1.0	5.9	10.3 ± 0.9	0.2
MUST-75	10.5 ± 1.0	10.1 ± 1.3	4.0	10.4 ± 1.3	0.4	9.8 ± 1.0	6.1	10.5 ± 1.0	0.2
MUST-76	4.7 ± 0.4	4.7 ± 0.6	0.7	5.0 ± 0.6	7.2	4.6 ± 0.5	2.7	4.8 ± 0.4	2.4
MUST-77	4.0 ± 0.4	3.9 ± 0.5	1.0	4.3 ± 0.5	8.8	3.8 ± 0.4	3.2	4.1 ± 0.4	3.2
MUST-78	4.2 ± 0.4	4.2 ± 0.5	0.7	4.6 ± 0.6	9.0	4.1 ± 0.4	3.0	4.3 ± 0.4	2.9
MUST-79	4.0 ± 0.4	3.9 ± 0.5	1.0	4.3 ± 0.5	8.8	3.8 ± 0.4	3.2	4.1 ± 0.4	3.2
MUST-80	40.3 ± 3.7	33.7 ± 4.2	16.4	33.2 ± 4.1	17.6	32.6 ± 3.4	19.1	37.2 ± 3.3	7.6
MUST-81	26.5 ± 2.4	23.3 ± 2.8	12.2	23.2 ± 2.8	12.6	22.6 ± 2.3	14.6	25.5 ± 2.3	3.9
MUST-82	78.9 ± 7.1	63.6 ± 7.7	19.4	62.3 ± 7.6	21.1	61.0 ± 6.2	22.7	71.9 ± 6.3	8.9
MUST-83	21.9 ± 2.0	19.7 ± 2.4	10.0	19.8 ± 2.4	9.8	19.2 ± 2.0	12.3	21.4 ± 1.9	2.5
MUST-84	60.7 ± 5.5	48.6 ± 5.9	20.0	47.6 ± 5.8	21.5	46.3 ± 4.7	23.6	55.3 ± 4.9	8.8
MUST-90	112.7 ± 10.2	90.2 ± 11.1	19.9	87.9 ± 10.7	22.0	86.4 ± 8.8	23.3	101.6 ± 9.0	9.9
MUST-91	25.0 ± 2.3	22.2 ± 2.7	11.2	22.1 ± 2.7	11.4	21.6 ± 2.2	13.6	24.1 ± 2.1	3.5
MUST-92	65.4 ± 6.2	52.6 ± 6.6	19.6	51.5 ± 6.4	21.3	50.0 ± 5.3	23.6	60.0 ± 5.6	8.3
KONG_1	14.8 ± 1.4	14.5 ± 1.8	2.1	14.8 ± 1.8	0.3	14.2 ± 1.5	4.1	14.8 ± 1.3	0.2
KONG_2	25.7 ± 2.3	23.7 ± 2.9	7.8	23.7 ± 2.9	7.9	23.1 ± 2.4	10.1	24.8 ± 2.2	3.5
KONG_3	17.4 ± 1.6	16.7 ± 2.0	4.2	16.9 ± 2.1	3.1	16.4 ± 1.7	6.2	17.2 ± 1.5	1.2

KONG_4	29.2 ±2.7	26.5 ± 3.2	9.1	26.4 ± 3.2	9.5	25.8 ± 2.6	11.6	27.9 ± 2.5	4.4
KONG_5	11.1± 1.0	11.1 ± 1.4	0.1	11.4 ± 1.4	3.1	10.9 ± 1.1	2.1	11.1 ± 1.0	0.2
KONG_6	11.2 ± 1.0	11.2 ± 1.4	0.2	11.6 ± 1.4	2.9	11.0 ± 1.1	2.1	11.2 ± 1.0	0.2
KONG_7	11.4 ± 1.0	11.3 ± 1.4	0.3	11.7 ± 1.4	2.8	11.1 ± 1.1	2.3	11.4 ± 1.0	0.2
KONG_8	6.8 ± 0.6	7.0 ± 0.9	3.1	7.4 ± 0.9	10.1	6.8 ± 0.7	0.7	6.8 ± 0.6	0.3
KONG_9	6.7 ± 0.6	6.9 ± 0.8	3.0	7.3 ± 0.9	10.1	6.7 ± 0.7	0.5	6.7 ± 0.6	0.4
KONG_10	6.8 ± 0.6	7.0 ± 0.9	3.1	7.5 ± 0.9	10.0	6.9 ± 0.7	0.9	6.8 ± 0.6	0.2
KONG_11	6.8 ± 0.6	7.0 ± 0.9	3.1	7.5 ± 0.9	10.1	6.8 ± 0.7	0.8	6.8 ± 0.6	0.3
KONG_12	7.0 ± 0.6	7.2 ± 0.9	3.1	7.6 ± 0.9	9.7	7.0 ± 0.7	0.9	7.0 ± 0.6	0.1
KONG_13	6.7 ± 0.7	6.9 ± 0.9	3.0	7.4 ± 1.0	10.0	6.8 ± 0.7	0.6	6.8 ± 0.7	0.3
KONG_14	1.4 ± 0.2	1.4 ± 0.2	0.1	1.6 ± 0.2	10.6	1.4 ± 0.2	2.0	1.5 ± 0.2	4.8
KONG_15	0.8 ± 0.1	0.8 ± 0.2	4.1	0.8 ± 0.2	7.4	0.8 ± 0.2	2.5	0.8 ± 0.2	8.6
KONG_16	1.4 ± 0.2	1.4 ± 0.2	0.0	1.5 ± 0.2	10.0	1.4 ± 0.2	1.9	1.5 ± 0.2	4.9
KONG_17	1.2 ± 0.2	1.2 ± 0.2	0.9	1.3 ± 0.2	8.9	1.2 ± 0.2	0.9	1.2 ± 0.2	5.9
KONG_18	3.5 ± 0.3	3.6 ± 0.4	1.2	3.9 ± 0.5	10.6	3.5 ± 0.4	0.9	3.7 ± 0.3	3.7
KONG_19	3.4 ± 0.3	3.5 ± 0.4	1.3	3.8 ± 0.5	10.7	3.4 ± 0.4	0.6	3.6 ± 0.3	3.9
KONG_20	3.3 ± 0.3	3.4 ± 0.4	1.6	3.7 ± 0.5	10.8	3.3 ± 0.4	0.3	3.5 ± 0.3	4.0
KONG_21	0.9 ± 0.1	0.9 ± 0.1	3.8	0.9 ± 0.1	8.4	0.9 ± 0.1	2.2	0.9 ± 0.1	7.9
KONG_22	4.5 ± 0.4	4.6 ± 0.6	1.8	5.0 ± 0.6	10.0	4.5 ± 0.5	0.1	4.6 ± 0.4	2.5
KONG_23	2.8 ± 0.3	2.9 ± 0.4	3.6	3.2 ± 0.4	13.7	2.9 ± 0.3	1.7	3.0 ± 0.3	5.0
KONG_24	1.5 ± 0.2	1.5 ± 0.2	0.9	1.7 ± 0.2	12.7	1.5 ± 0.2	1.1	1.5 ± 0.2	4.8
KONG_25	3.3 ± 0.3	3.4 ± 0.4	2.1	3.7 ± 0.5	11.3	3.3 ± 0.3	0.2	3.4 ± 0.3	4.1
KONG_26	3.3 ± 0.3	3.4 ± 0.4	2.1	3.7 ± 0.5	11.3	3.3 ± 0.3	0.3	3.4 ± 0.3	4.1
KONG_27	2.3 ± 0.2	2.4 ± 0.3	4.4	2.7 ± 0.4	17.5	2.4 ± 0.3	2.3	2.4 ± 0.2	5.7
KONG_28	1.1 ± 0.1	1.2 ± 0.2	2.3	1.2 ± 0.2	10.0	1.1 ± 0.1	0.5	1.2 ± 0.1	6.1
KONG_29	29.2 ± 2.7	26.4 ± 3.3	9.4	26.3 ± 3.2	9.8	25.7 ± 2.6	11.8	27.9 ± 2.5	4.4
KONG_30	57.3 ± 5.2	48.1 ± 5.9	16.0	47.5 ± 5.8	17.1	46.1 ± 4.7	19.5	52.2 ± 4.7	8.8
KONG_31	N.A.								
KONG_32	N.A.								
KONG_33	N.A.								
KONG_34	N.A.								
KONG_35	0.8 ± 0.2	0.8 ± 0.2	9.4	0.9 ± 0.2	13.0	0.8 ± 0.2	8.0	0.8 ± 0.2	8.7
KONG_36	1.3 ± 0.2	1.4 ± 0.2	5.7	1.5 ± 0.3	15.6	1.4 ± 0.2	4.0	1.4 ± 0.2	5.1

KONG_37	1.5 ± 0.2	1.5 ± 0.2	5.8	1.7 ± 0.3	17.4	1.5 ± 0.2	3.8	1.5 ± 0.2	4.8
KONG_38	0.9 ± 0.2	1.0 ± 0.2	8.1	1.0 ± 0.2	13.3	1.0 ± 0.2	6.7	1.0 ± 0.2	7.6
KONG_39	N.A.								
KONG_40	N.A.								
KONG_41	0.4 ± 0.1	0.4 ± 0.2	17.2	0.4 ± 0.2	13.9	0.4 ± 0.2	16.1	0.4 ± 0.2	13.0

* Lal (1991) and Stone (2000) scaling schemes are used.
† Various scaling schemes are used for time-dependent production.
§ Age difference is calculated between age from time-constant production scheme and various time-dependent production schemes.
N.A. means not available.
All the exposure ages are cited as ka.

References

Desilets, D., and Zreda, M., 2006, Elevation dependence of cosmogenic 36Cl production in Hawaiian lava flows, Earth and Planetary Science Letters, v. 246, p. 277-287.

Desilets, D., and Zreda, M., 2003, Spatial and temporal distribution of secondary cosmic-ray nucleon intensities and applications to in situ cosmogenic dating, Earth and Planetary Science Letters, v. 206, p. 21-42.

Dunai, T.J., 2000, Scaling factors for production rates of in situ produced cosmogenic nuclides: a critical reevaluation: Earth and Planetary Science Letters, v. 176, p. 157-169.

Guyodo, Y., and Valet, J.P., 1999, Global changes in intensity of the Earth's magnetic field during the past 800 kyr, Nature, v. 399, p. 249-252.

Lal, D., 1991, Cosmic ray labeling of erosion surfaces: in situ nuclide production rates and erosion models: Earth and Planetary Science Letters, v. 104, p. 429-439.

Lifton, N. A, Bieber, J.W., Clem, J.M., Duldig, M.L., Evenson, P., Humble, J.E., and Pyle, R., 2005, Addressing solar modulation and long-term uncertainties in scaling secondary cosmic rays for in situ cosmogenic nuclide applications, Earth and Planetary Science Letters, v. 239, p. 140-161.

Ohno, M., Hamano, Y., 1992, Geomagnetic poles over the past 10,000 years, Geophysical Research Letters, v. 19, p. 1715-1718.

Ono, Y., Liu, D., and Zhao, Y., 1997, Paleoenvironment of Tibetan Plateau from glacial fluctuations in the northern foot of the West Kunlun Mountains: Journal of Geography (in Japanese), v. 106, p. 184-198.

Stone, J.O., 2000, Air pressure and cosmogenic isotope production: Journal of Geophysical Research, v. 105, no. B10, p. 23753–23759.

Yang, S., Odah, H., Shaw, J., Variations in the geomagnetic dipole movement over the last 12,000 years, Geophysical Journal International, v. 140, 158-162.

http://hess.ess.washington.edu/math/, CRONUS Earth 2.